



Synergistic Effects of Nano-zinc Oxide on Improving the Flame Retardancy of EVA Composites with an Efficient Triazine-Based Charring Agent

Bo Xu^{1,2} · Wen Ma^{1,2} · Xiaolu Bi³ · Lushan Shao^{1,2} · Lijun Qian^{1,2}

Published online: 6 March 2019

© Springer Science+Business Media, LLC, part of Springer Nature 2019

Abstract

The synergistic effect of nano-zinc oxide (nano-ZnO) on the flame retardancy and thermal stability of intumescent flame retardant ethylene–vinyl acetate (EVA/IFR) consisting of novel hyperbranched triazine-based charring agent (HTCFA) and APP was evaluated by limiting oxygen index (LOI), UL-94 measurement, cone calorimeter test (CCT) and thermogravimetric analysis (TGA), and the residue analysis was also carried out through scanning electron microscopy (SEM), fourier transform infrared (FTIR), laser raman spectroscopy (LRS), and X-ray photoelectron spectroscopy (XPS). The results showed that introducing a certain amount of nano-ZnO could obviously enhance LOI value and UL-94 rating, and effectively restrain the combustion performance of EVA/IFR composites, leading to the decrease of heat and smoke release. The addition of 0.5 wt% nano-ZnO into EVA/IFR composite obtained the highest catalytic effectivity (CAT-EFF). TGA results uncovered a distinct synergistic carbonization effect existed between nano-ZnO and IFR, and nano-ZnO could obviously improve the high-temperature thermal stability and promote the char formation of IFR and EVA/IFR. Analysis of final char residues proved that the incorporation of appropriate amount of nano-ZnO contributed to remaining more P and forming more high-quality graphitization char layers with richer P–O–C and P–N cross-linking structures in condensed phase owing to the catalytic carbonization effect of nano-ZnO on IFR system, which played a critical role in remarkable improvement of flame retardancy and smoke suppression properties of composites.

Keywords EVA · Intumescent flame retardancy · Zinc oxide · Triazine-based char-forming agent · Synergistic effect

Introduction

Ethylene–vinyl acetate (EVA) is a copolymer with good physical and mechanical properties that has been widely applied in many fields. However, like most organic polymers,

EVA is also inherently inflammable with a high smoke emission and thus its applications have been restricted due to the terrible fire-resistance [1, 2]. Intumescent flame retardant (IFR) systems have been commonly regarded as an efficient way to enhance the flame-resistance of polymer materials because of the characteristic of low toxicity, low corrosion, low smoke and excellent char-forming ability, which would be a potential candidate for substituting halogen-containing flame retardants [3–5].

However, IFRs are always with low flame retardant efficiency and the large addition must be required for obtaining good flame-retardant properties, which certainly decreases polymer materials' comprehensive performance. To enhance the flame retardant efficiency of IFR in polymers, zeolites [6], transition metal oxides [7], metal compounds [8], organic boron siloxane [9, 10] and the like have been used as flame-retardant synergistic agents. For instance, the synergistic effect of transition metal oxides on polymer/IFR systems have been widely investigated, such as metal oxides of

✉ Bo Xu
xubo@btbu.edu.cn

✉ Lijun Qian
qianlj@th.btbu.edu.cn

¹ School of Materials Science and Mechanical Engineering, Beijing Technology and Business University, Fucheng Road 11, Beijing 100048, People's Republic of China

² Beijing Key Laboratory of Quality Evaluation Technology for Hygiene and Safety of Plastics, Beijing Technology and Business University, Fucheng Road 11, Beijing 100048, People's Republic of China

³ Chongqing Hongyu Precision Industrial Co., LTD, Hongyu Road 9, Chongqing 402760, People's Republic of China

Zn, Ti and Ni in intumescent flame retardant polypropylene system by Cai et al. [11] and Yang et al. [12], oxides of Fe and La in EVA/IFR systems, ZnO in silicone rubber/IFR systems by Chen et al. [13] and so on. These results revealed that transition metal oxides as synergists could effectively promoted forming high-quality char layers with good mechanical strengths and thermal stabilities through catalyzing cross-linked reactions in IFR system.

In the previous work, our lab has prepared a hyper-branched triazine-based char-forming agent (HTCFA) showing good thermal stability, and it has been applied to an innovated IFR system with APP, which showed excellent flame retardancy in PP matrix [14]. In this work, nano-ZnO was selected as a synergist and its impact on combustion behavior and thermal decomposition properties of EVA/IFR system based on HTCFA and APP have been investigated by LOI, UL-94, CCT, TGA and residue analysis (SEM, FTIR, LRS and XPS).

Experimental

Materials

EVA containing 17.6–20.4 wt% vinyl acetate units was bought from BASF-YPC CO., Ltd. (Nanjing, China). APP ($n > 1000$) was produced by Polyrocks Chemical Co. Ltd, China. HTCFA was prepared in our lab [14] and Scheme 1 shows its structure. Nano-zinc oxide ($\geq 99.9\%$ metals basis, 30 ± 10 nm) was provided by Sinopharm Chemical Reagent Co., Ltd., China.

Preparation of Composites

EVA and all the additives were dried in vacuum at 80°C for 12 h before processing. EVA samples were melt-mixed via a torque rheometer (KX-160, Jiangsu, China) with the process temperature of 130°C and the rotation speed of 40 r/min. Then, they were hot-pressed to produce sheets with standard sizes of subsequent tests. The formulations are presented in Table 1. The loading of IFR was fixed at 25 wt% with the weight ratio of APP and HTCFA 3:1, which showed the optimum flame retardant performance in our previous work [15].

Scheme 1 The structure of HTCFA

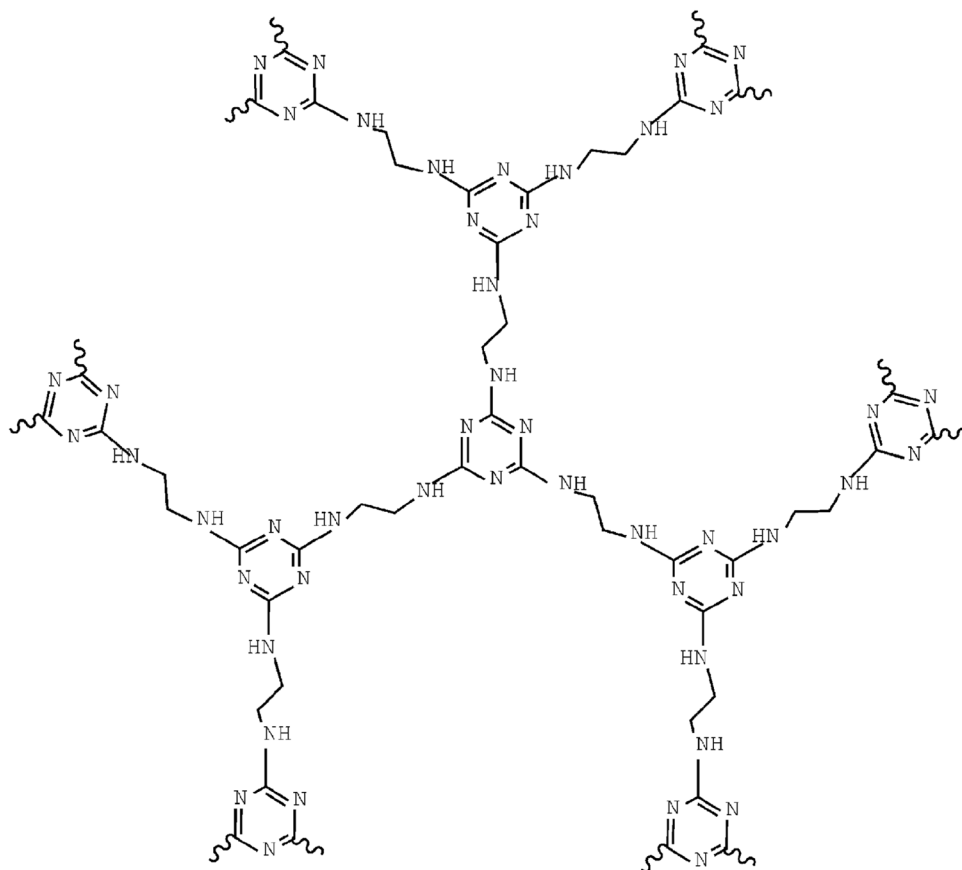


Table 1 Formulation of neat EVA and EVA composites and catalytic effects of nano-ZnO

Samples	EVA /phr ^a	IFR ^b /phr	Nano-ZnO/phr	LOI (%)	Δ LOI (%) ^c	wt (Zn) (%) ^d	CAT-EFF ^e
EVA	100	–	–	–	–	–	–
EVA/IFR	75	25	–	25.2	–	–	–
EVA/IFR/0.25ZnO	75	25	0.25	27.3	2.1	0.20	10.50
EVA/IFR/0.5ZnO	75	25	0.5	29.5	4.3	0.40	10.75
EVA/IFR/0.75ZnO	75	25	0.75	28.6	3.4	0.60	5.67
EVA/IFR/1ZnO	75	25	1.0	27.0	1.8	0.80	2.25

^aParts per hundred EVA/IFR^bIFR means the mass ratio between APP and HTCFA was 3:1^c Δ LOI (%) means the difference of LOI between EVA/IFR/ZnO composites and EVA/IFR^dwt(Zn) (%) means Zn concentration in EVA/IFR/ZnO^eCAT-EFF = Δ LOI/wt(Zn) (1)

Instruments and Characterization

LOI values were measured using a FTT 0080 LOI instrument (Fire Testing Technology Ltd. (FTT), UK) according to American Society for Testing and Materials (ASTM) D2863-17 and the sample dimension was 130 mm × 6.5 mm × 3.2 mm. UL-94 vertical burning rating tests were performed by an FTT0082 tester (FTT, UK) following the procedures in ASTM D3801-10 (sample dimension: 125 mm × 12.7 mm × 3.2 mm). The forced combustion behaviour was measured by an FTT0007 cone calorimetry (FTT, UK) according to ISO 5660-1 with an external heat flux of 50 kW/m² (sample dimension: 100 mm × 100 mm × 3 mm).

Fourier transform infrared (FTIR) spectra of residues after cone test were recorded by a Nicolet 6700 FTIR spectrometer (Nicolet, USA) with KBr pellets.

TGA tests were performed on a TGA instrument thermal analyzer (TA Q50, USA). About 2–5 mg of a tested sample was heated from 50 to 700 °C under neat N₂ atmosphere at rate of 20 °C/min.

The morphologies of the char were observed in a FEI Quanta 250 FEG field-emission SEM with a voltage of 20 kV. LRS spectra were obtained from a LabRAM HR Evolution Raman spectrometer (HORIBA, Japan) with excitation by a 532 nm helium–neon laser line and scanning in the scope of 50–4000 cm⁻¹. XPS spectra were recorded by a PHI Quantera-II SXM (Ulvac-PHI, Japan) using Al K α excitation radiation (X-ray power of 2.5 kW).

Results and Discussion

Flammability of EVA Composites

Flammability properties of EVA composites were tested by limiting oxygen index and vertical flammability tests.

Figure 1 shows the impact on LOI and UL-94 rating results of EVA/IFR composites when adding diverse contents of nano-ZnO. EVA/IFR composite only attained a LOI value of 25.2% and reached UL-94V-2 rating. However, the flame retardancy of EVA/IFR composites was significantly improved after combining nano-ZnO. It could be observed that the LOI values of EVA/IFR/ZnO systems initially went up rapidly with increasing the nano-ZnO loadings and then decreased with the nano-ZnO concentration more than 0.5 wt%. When adding 0.5 wt% nano-ZnO, LOI reached the highest value of 29.5% and UL-94V-0 rating was obtained. And all the composites containing nano-ZnO could reach UL-94V-0 rating. As a result, it indicated that there was an appropriate loading amount of nano-ZnO, with which IFR and nano-ZnO gave the optimal flame retardant synergistic effect on EVA. The higher content of nano-ZnO might break the harmony between expansion behavior and char-forming

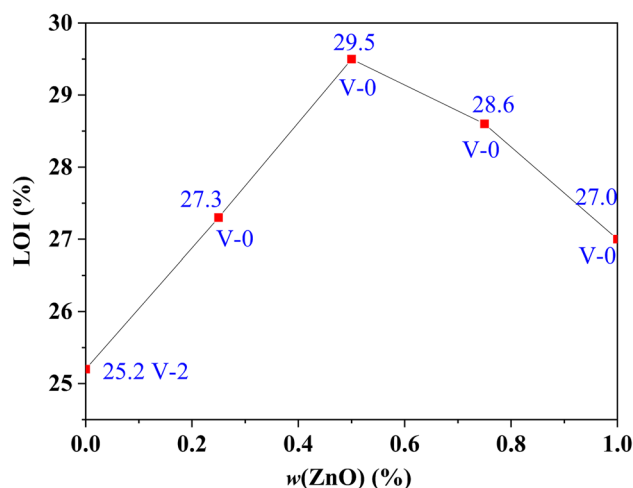


Fig. 1 Effect of nano-ZnO on the flame retardant properties of EVA/IFR composites

function of EVA/IFR/ZnO composites. Therewith the action mechanism would be analyzed subsequently.

Catalytic Effects of Nano-ZnO

The catalytic efficiency (CAT-EFF) of nano-ZnO on EVA/IFR composites, defined as the LOI augments caused by per weight percent of Zn [16], was calculated based on Formulation provided in Table 1 footnote and it shows the CAT-EFF results. The CAT-EFF values for EVA/IFR/ZnO composites increased at first and then reduced subsequently with increasing the nano-ZnO concentration, which was similar with LOI results. When the nano-ZnO loading was 0.5 wt%, the highest CAT-EFF value (10.75) was obtained, which also possessed the highest LOI value. Therefore, 0.5 wt% loading of nano-ZnO was the most effective for EVA/IFR systems, which would be chosen as the subject to be further investigated.

Forced Combustion Behaviour of EVA/IFR/ZnO Composites

Cone calorimetry was a superior measurement method for studying the combustion behaviour of materials. Table 2 summarized the important parameters which were used to

describe the characteristics of pure EVA and EVA composites during combustion.

Figure 2 shows the heat release rate (HRR) and total heat release (THR) curves of EVA, EVA/IFR and EVA/IFR/0.5ZnO. As shown in Fig. 2, pure EVA burned quickly after ignition, and a HRR peak of 1758 kW/m² occurred at about 150 s. As far as EVA/IFR and EVA/IFR/0.5ZnO, both HRR values showed two main peaks. The first stage was attributed to the decomposition of the IFR, and thereafter cross-linking structures formed a preliminary covering on the surface of matrix material. Its low viscosity and terrible strength were not enough to block the generated gas to make the char layer expand, and the ability to block heat release was limited inevitably. As accumulated, the char layer began to swell, but it was not strong enough to prevent from being undone by a steady stream of gases, so the second phase appeared. Fortunately, as the old char layer was destroyed, the new one swelled immediately. Over time, the expanded carbon layer became stronger and stronger, once again effectively blocking the release of heat. It was obvious that the peak2-HRR value of EVA/IFR/0.5ZnO was smaller than that of EVA/IFR. Furthermore, the THR value of EVA/IFR was much lower than pure EVA (136 MJ/m²) and the value of EVA/IFR/0.5ZnO presented a further lower THR value with the addition of nano-ZnO. Also, it was worth noting

Table 2 Cone calorimetry data of EVA composites

Sample	TTI (s)	Peak1-HRR (kW/m ²)	Peak2-HRR (kW/m ²)	THR (MJ/m ²)	Peak-COP (10 ⁻³ g/s)	Peak-CO ₂ P (10 ⁻¹ g/s)	Peak-SPR (10 ⁻² m ² /s)	TSP (m ²)	Residue (wt%)
EVA	36	1758	–	136	17.3	9.6	20.88	32.8	0
EVA/IFR	27	315	328	97	5.4	1.8	7.75	16.9	20.2
EVA/IFR/0.5ZnO	28	305	247	90	4.1	1.5	5.81	15.5	23.4

Peak1-HRR and Peak2-HRR: the first and second peak value on the heat release rate (HRR) curves, respectively

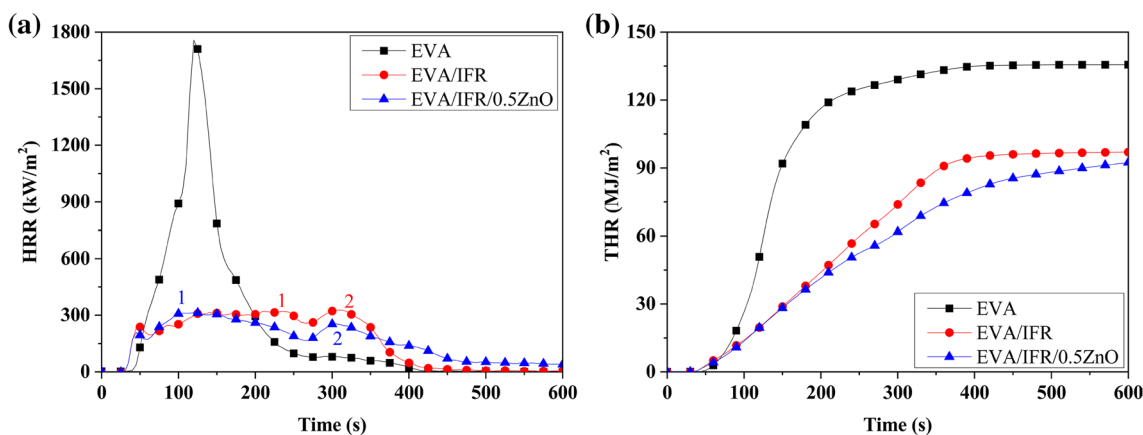


Fig. 2 HRR (a) and THR (b) curves of EVA, EVA/IFR and EVA/IFR/0.5ZnO

that the THR curve of EVA/IFR was steeper than that of EVA/IFR/0.5ZnO from 220 to 350 s which corresponded to the main decomposition process of the composite, and then tended to be flat. That was to say, EVA/IFR without ZnO reached the maximum heat release value earlier than that with nano-ZnO and thus the former presented the stronger combustion intensity. This result could be explained by the fact that the presence of nanometer zinc oxide improved the quality of the char layer which was more continuous and denser, resulting in the longer heat release duration, even if it began to form a little later (Table 3).

From Table 2, it was not difficult to find the time to ignition (TTI) with addition of IFR or IFR/0.5ZnO was obviously shortened. It was reported that the pyrolysis of EVA started from the deacetylation of VA monomers [17], and APP could accelerated the decomposition [18]. Also, the existence of ZnO could further catalyze the pyrolysis process.

Figure 3 gives the smoke production rate (SPR) and smoke release product (TSP) curves of composites. It was found that with adding IFR and IFR/0.5ZnO into EVA, all the peak-SPR (PSPR) values significantly decreased compared to neat copolymer. Especially, it reduced from 0.206 m²/s for EVA to 0.077 m²/s and 0.058 m²/s, with 62.8% and 72.0% reduction when adding IFR and IFR/0.5ZnO and the PSPR of EVA/IFR/0.5ZnO appeared obviously later than EVA/IFR. This indicated that the presence of nano-ZnO in IFR

inhibited the smoke production rate of composites. For TSP, the value of EVA/APP/0.5ZnO was slightly lower than EVA/IFR but much lower than neat EVA, which suggested EVA/IFR combining nano-ZnO possessed more excellent smoke suppression properties.

The emission of toxic gas (CO) and CO₂ was assessed and Fig. 4 shows the product curves of CO (COP) and CO₂ (CO₂P) which are similar with the HRR curves. With adding IFR and IFR/0.5ZnO into EVA, all the generations of CO and CO₂ were restrained. Still, the combination of IFR and nano-ZnO could more efficiently inhibit forming CO and CO₂ during combustion of composites. This also was attributed to the formation of firm charred layer protecting the underlying polymer from burning.

Figure 5 gives the mass loss curves of EVA and EVA composites during burning, and the char residues are also listed in Table 2. Neat EVA lost its mass much faster than EVA/IFR and EVA/IFR/0.5ZnO and remained nothing at the end. Further, it was also obvious that much more residues were obtained (23.4 wt%) after nano-ZnO combined with IFR, which indicated that nanometre zinc oxide could promote the formation of the stable expansive char crust, prohibited transmitting heat and combustible gas generated from burning as mentioned above.

Digital photographs of the residues after cone calorimeter test are displayed in Fig. 6. Obviously, both EVA/IFR and EVA/IFR/ZnO composites formed swollen and dense char, yet a few of tiny holes and cracks were found on the outer surface labelled using ovals in Fig. 6a for EVA/IFR char, bringing the weaker barrier effect of char. It was surprising that the presence of 0.5 wt% nano-ZnO in composites significantly promoted forming homogeneous and compact char residues without visible holes on the surface, as shown from Fig. 6b. High-quality intumescent char layers could play a key role in preventing the transfer of heat/combustible

Table 3 TGA data of IFR with and without nano-ZnO under nitrogen

Sample	$T_{5\%}$ (°C)	T_{peak} (°C)	Char residue (%)		
			500 °C	600 °C	700 °C
IFR	324	446	57.9	51.1	46.8
IFR/0.5ZnO	310	416	61.8	56.6	53.5
IFR/0.5ZnO-Cal	325	447	58.7	52.1	47.9

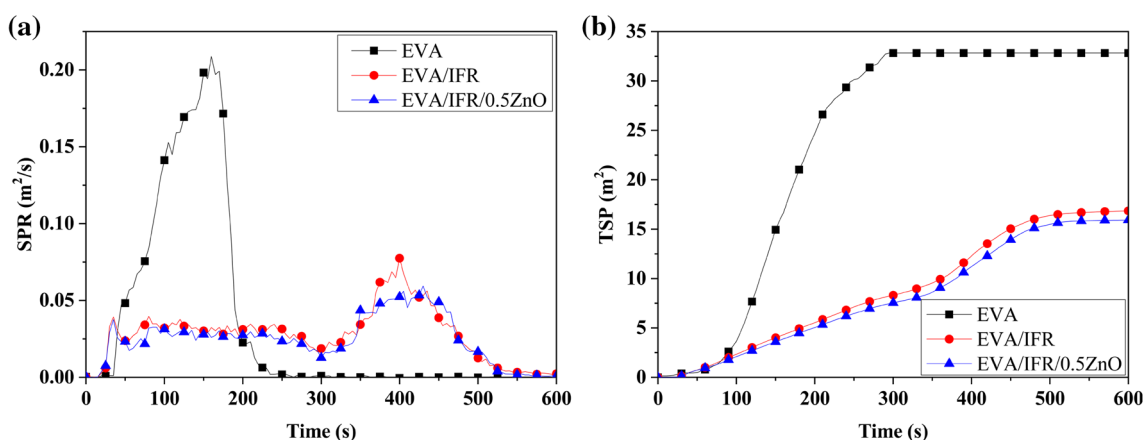


Fig. 3 SPR (a) and TSP (b) curves of EVA, EVA/IFR and EVA/IFR/0.5ZnO

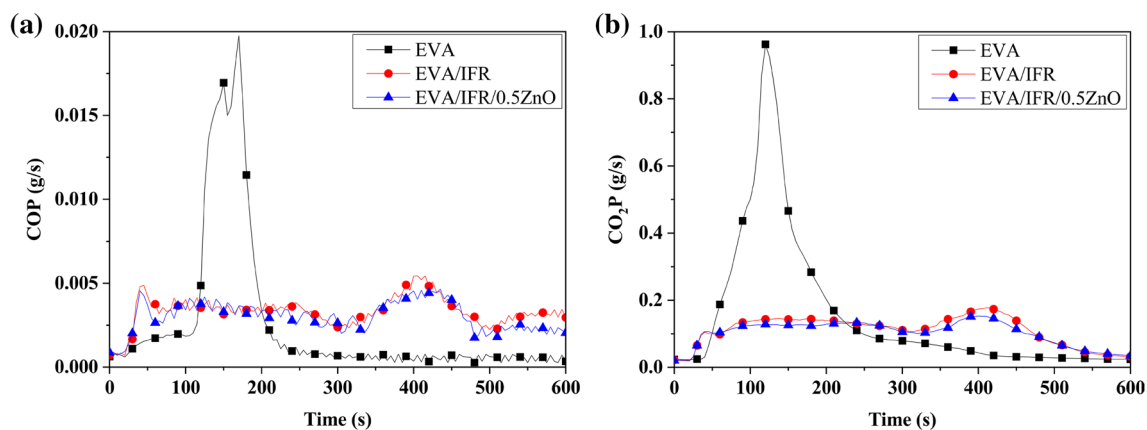


Fig. 4 COP (a) and CO_2P (b) curves of EVA, EVA/IFR and EVA/IFR/0.5ZnO

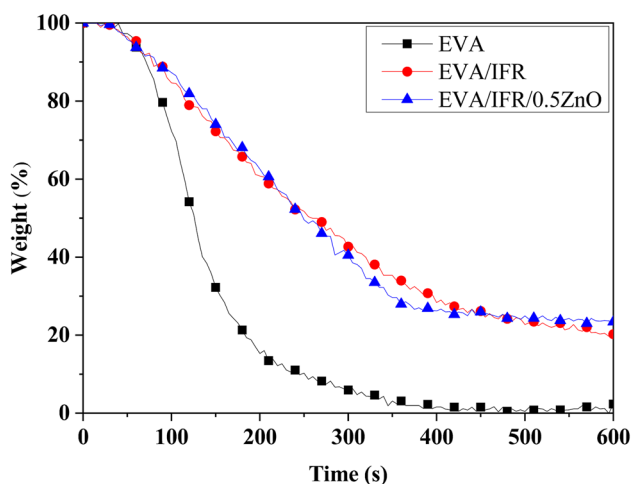


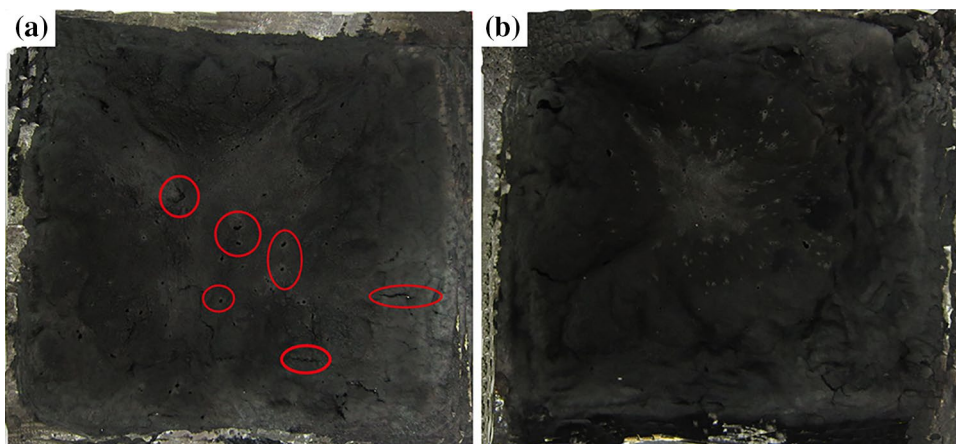
Fig. 5 The residue mass curves of EVA, EVA/IFR and EVA/IFR/0.5ZnO composites

gas, consequently improving the flame resistance of EVA composites.

Thermogravimetric Analysis

Thermogravimetric analysis was used to rapidly evaluate the thermal degradation behaviour and charring ability of IFR and IFR/0.5ZnO. TGA and DTG curves are present in Fig. 7, and the data are collected in Table 2. It could be seen that IFR possessed great thermal stability, whose initial decomposition temperature was 324 °C based on 5 wt% mass loss ($T_{5\%}$). The thermal decomposition course of IFR was split into three stages. As for the first step, it might be attributed to the release of water, ammonia and cross-linked polyphosphoric acids which occurred at 305 °C. The second one appeared at 446 °C and was the main decomposition process, resulting from the disintegration and formation of char. The last peak occurred at 660 °C and was attributed to the decomposition of char residue. However, the combination with nano-ZnO did affect the degradation behaviour of IFR system and there was an apparent synergistic effect between

Fig. 6 Digital photos of chars of EVA/IFR (a) and EVA/IFR/0.5ZnO (b)



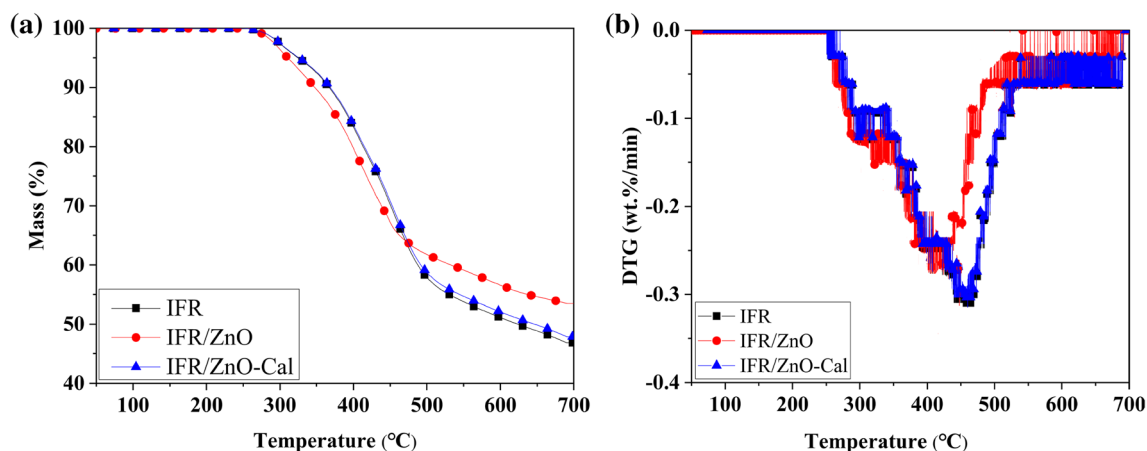


Fig. 7 TGA (a) and DTG (b) curves of IFR systems with and without nano-ZnO under N_2

them. The $T_{5\%}$ of IFR system lowered from 324 to 310 °C with the addition of nano-ZnO, which agreed with the previous results based on metal oxides system [11]. This was due to the fact that metal oxides could catalyze the amidation reactions between APP and HTCFA with the latter containing lots of imide groups, promoting forming char residues. In the curves of IFR/ZnO, it was found that the third peak was not evident and there were only two obvious decomposition steps, whose peaks occurred at 305 °C and 416 °C. This indicated that the existence of nano-ZnO could improve the char-forming ability and high-temperature thermal stability of IFR, testified by that the char residue of IFR/ZnO system was 61.8 wt%, 56.6 wt%, and 53.5 wt% at 500 °C, 600 °C, and 700 °C respectively, much higher than the corresponding values of IFR and IFR/ZnO calculation. Also, comparing the experimental thermal analysis curve of IFR/ZnO and the calculation one calculated based on the experimental values and mass fraction in IFR/ZnO system on the basis of Formula 1, some obvious differences occurred, especially

under high temperature (about > 450 °C). The third peak in the calculation DTG curve of IFR/ZnO still existed, which disappeared in the experimental curve. This revealed that the introduction of nano-ZnO could change the thermal degradation behaviour and enhance the thermal stability of APP/HTCFA system due to forming stable compounds or fragments under high temperature.

$$W_{\text{calculation}} = W_{\text{IFR}} \times 98.04\% + W_{\text{ZnO}} \times 1.96\% \quad (1)$$

Figure 8 presents the TGA and DTG curves of EVA and EVA composites under N_2 atmosphere and Table 4 listed the results. The EVA mass loss curve showed two degradation platforms. The first step could be explained by the elimination of the acetate side groups (deacetylation), leaving the polyenes and polymer chains with unsaturated bonds [19–21]. What's more, the second step could be ascribed to the cleavage of the polyenes in the form of alkyl at high temperatures to achieve complete thermal degradation. EVA began to go through thermal decomposition from

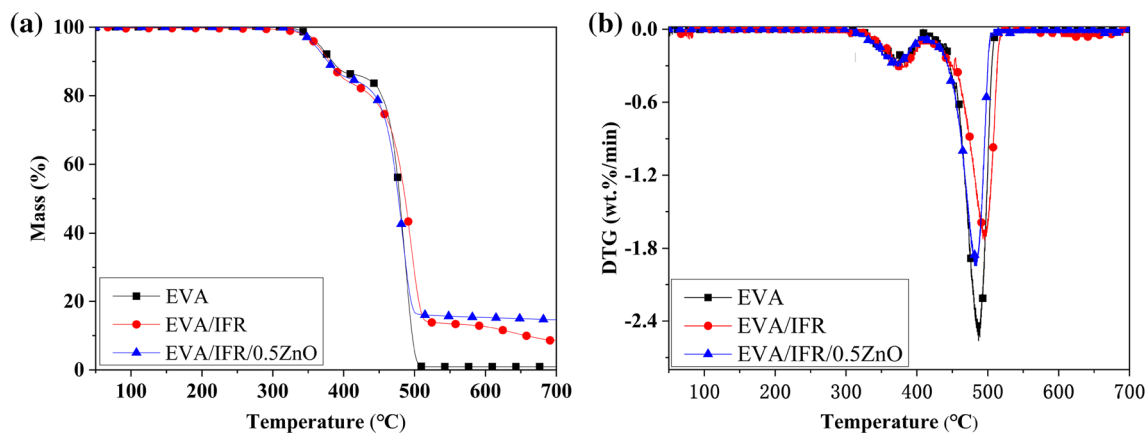


Fig. 8 TGA (a) and DTG (b) curves of EVA, EVA/IFR and EVA/IFR/0.5ZnO under N_2

Table 4 TGA data of EVA and EVA composites under N₂ and air atmosphere

Samples	N ₂ atmosphere			Air atmosphere		
	EVA	EVA/IFR	EVA/IFR/0.5ZnO	EVA	EVA/IFR	EVA/IFR/0.5ZnO
$T_{5\%}$ (°C)	365	362	358	346	345	346
T_{peak} (°C)	487	495	484	457	478	485
R_{peak} (%/min)	2.5	1.7	1.9	2.07	1.33	1.21
$W_{500^\circ\text{C}}$ (wt%)	4.5	28.4	16.9	4.46	21.82	24.64
$W_{600^\circ\text{C}}$ (wt%)	0	18.6	15.3	1.25	17.66	19.77
$W_{700^\circ\text{C}}$ (wt%)	0	8.6	14.7	0.1	10.9	13.5

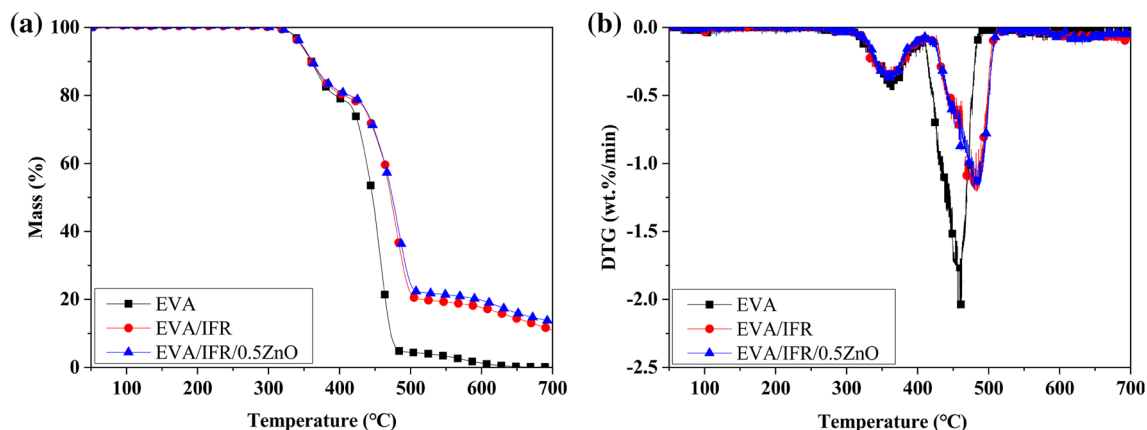
365 °C ($T_{5\%}$), and almost completely degraded up to 500 °C with nothing left at 700 °C. The addition of IFR to EVA at 25 wt% weight fraction led to a slight advance in the initial thermal degradation process of EVA. However, the thermal decomposition was transferred to high temperature and T_{peak} moved to 495 °C from 487 °C. Further, the char residues of EVA/IFR composite was significantly enhanced to 8.6 wt% at 700 °C. With the introduction of nano-ZnO into EVA/IFR, both $T_{5\%}$ and T_{peak} decreased and the char residues were remarkably improved with 15.3 wt% at 600 °C and 14.7 wt% at 700 °C. This indicated the presence of nano-ZnO promoted forming stable char residues at high temperature, effectively inhabiting the transfer of heat and diffusion of oxygen/inflammable volatiles.

Besides the thermal decomposition properties of EVA composites under N₂, the thermal oxidative degradation behaviour was also evaluated because polymer materials were practically used under air. Figure 9 gives the TGA and DTG curves under air atmosphere and the corresponding data are also listed in Table 4. Pure resin started to decompose from 346 °C, and there was only 0.1 wt% char left above 600 °C. After the addition of IFR or IFR/0.5ZnO into EVA, the degradation behaviour changed above about 400 °C with the better thermal stability and more char residues.

Moreover, the T_{peak} values of composites shifted to high temperature from 480 °C for EVA/IFR to 486 °C for EVA/IFR/0.5ZnO and yet the R_{peak} of the latter (1.21%/min) was lower than the former (1.33%/min). Also, the char residues obtained at 700 °C of EVA/IFR/0.5ZnO was 13.5 wt% which was much higher than those of EVA/IFR (10.9 wt%). These results indicated EVA/IFR/0.5ZnO also outperformed EVA/IFR in air atmosphere for the high-temperature thermal stability of residues, which could bring a better protective armor for under matrix in the real fire disaster.

Morphology Analysis of Char Residues

The micro-morphologies of the char layers after cone test for EVA/IFR and EVA/IFR/0.5ZnO were observed by SEM to further analyze the action mode of catalytic carbonization effect of nano-ZnO on the char-forming process of EVA composites. As shown in Fig. 10, when magnified 500 times, each sample (regardless of existing nano-ZnO) seemed to generate a continuous and complete surface, which was able to play a role as an isolation barrier in restricting transferring of oxygen/heat from underlying matrix. When magnified 1000 times, EVA/IFR system began to show its weakness, and some holes were clearly visible on the surface of

**Fig. 9** TGA (a) and DTG (b) curves of EVA and EVA composites under air

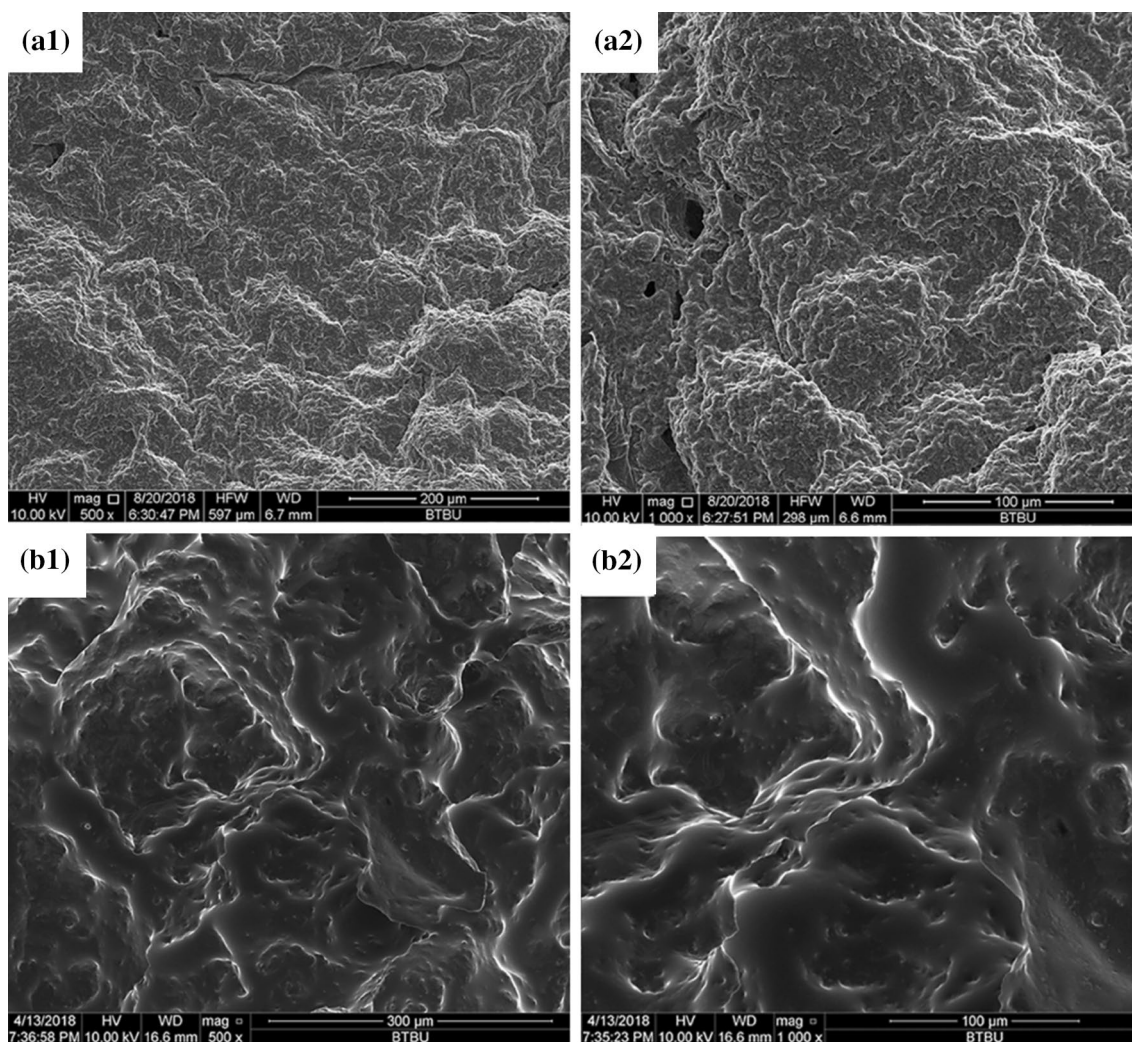


Fig. 10 SEM photographs of EVA/IFR (a1: $\times 500$, a2: $\times 1000$) and EVA/IFR/0.5ZnO (b1: $\times 500$, b2: $\times 1000$) char residues

the carbon residue, while EVA/IFR/0.5ZnO composite was still intact and solid. The results suggested that the combination of nano-ZnO into EVA/IFR produced the advantage of forming more cross-linked network structures, thus a more compact and tighter char layer occurred with better quality. Therefore, this kind of char layer contributed to the greater thermal stability, which was also revealed by TGA results very well.

Structure Analysis of the Char Residue

Figure 11 presents the Raman spectra of EVA/IFR and EVA/IFR/0.5ZnO residues after cone test to disclose the residue graphitization structure. There were two characteristic bands to be noted in the spectra: *D* band ($\sim 1360\text{ cm}^{-1}$) and *G* band ($\sim 1580\text{ cm}^{-1}$), which correspond to the vibration of amorphous or unorganized and graphitic structures of carbon materials, respectively. The integral peak area ratio of *D*

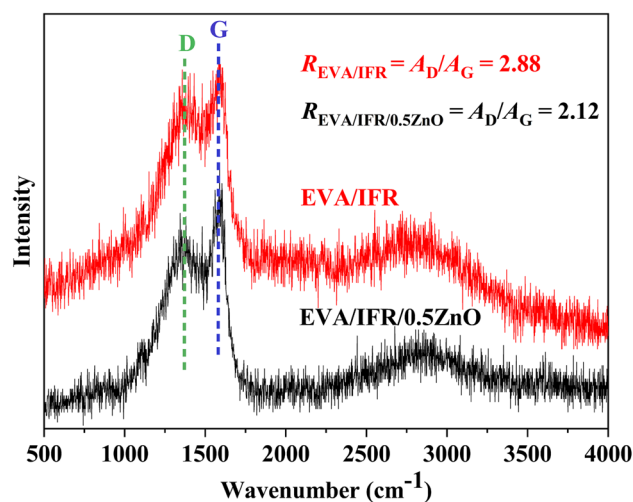


Fig. 11 Raman spectra of EVA/IFR and EVA/IFR/0.5ZnO char residues

band and G band, $R = A_D/A_G$, could well reflect the graphitization degree and was inversely proportional to an in-plane microcrystalline size of carbon materials. The lower R value indicated a higher graphitization degree of residues and the matrix would obtain a better shield protection from burning [22–24]. As seen from Fig. 11, the R values for EVA/IFR and EVA/IFR/0.5ZnO were 2.88 and 2.12 respectively, meaning that EVA/IFR/0.5ZnO residues possessed richer graphitic structure, while EVA/IFR char layer contained less graphitic structure. Raman analysis results further manifested the introduction of nano-ZnO could accelerate the EVA/IFR composite forming higher graphitization-degree char residues, more effectively protecting the composites against burning and hence leading to better flame retardancy for EVA/IFR/ZnO composite.

Composition Analysis of Char Residues

FTIR spectra of char residues after cone test for EVA/IFR-3 and EVA/IFR-6 are presented in Fig. 12, which could be used to investigate the chemical composition. The spectra showed typical characteristic peak at 3118 cm^{-1} belonged to $-\text{OH}$ and the absorption peak at about 1638 cm^{-1} was attributed to polyaromatic $\text{C}=\text{C}$ structure [25]. Band appeared at 1400 cm^{-1} was attributed to $\text{P}-\text{N}$ structure, and meanwhile the absorption peak located at 1002 cm^{-1} should be the corresponding

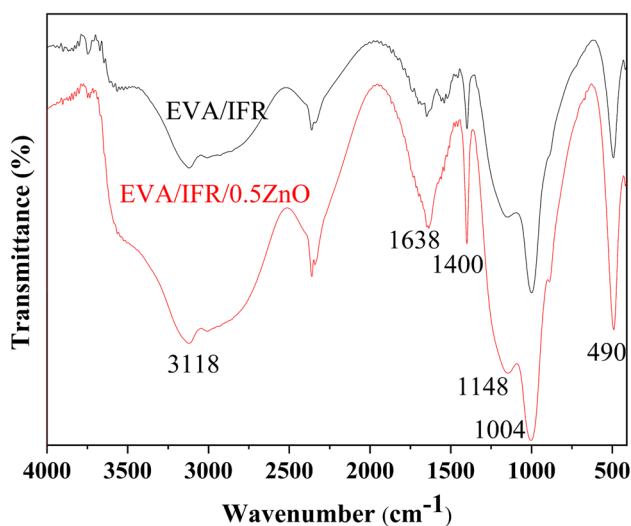


Fig. 12 FTIR spectra of EVA/IFR and EVA/IFR/0.5ZnO char residues

contribution of the stretching vibration of $\text{C}-\text{O}-\text{P}$ structure [25]. The above FTIR spectra revealed that there were abundant $\text{C}-\text{O}-\text{P}$ and $\text{P}-\text{N}$ structures existing in residues, indicating that cross-linked reactions took place between APP and HTCFA [26] and consequently phosphorous-containing polyaromatic residues formed during burning. The type of chars could result in a superior barrier to prevent effectively the material from degrading. Furthermore, comparing the two FTIR spectra, the characteristic peaks for EVA/IFR/ZnO at 1400 cm^{-1} and 1004 cm^{-1} , corresponding to $\text{P}-\text{N}$ and $\text{P}-\text{O}-\text{C}$ structures, showed quite higher intensity than EVA/IFR, which may be due to the reactions between nano-ZnO and APP, remaining more polyphosphoric acid to react with the char-formation agent HTCFA in condensed phase. This also explained why EVA/IFR/ZnO possessed higher-quality char residues as mentioned above.

XPS spectra could analyze the surface chemical structure of condensed phase [27]. The element concentrations in residues after cone test are listed in Table 5. Obviously, the results showed nano-ZnO was beneficial to lock more P and O in condensed phase during combustion of EVA/IFR composite, which could effectively strengthen the char quality as discussed earlier.

Meanwhile, $\text{C}1s$, $\text{O}1s$, $\text{N}1s$ and $\text{P}2p$ spectra of EVA/IFR and EVA/IFR/0.5ZnO residues are shown in Figs. 13, 14, 15 and 16 and the fitting results are listed in Table 6. From Fig. 13, the binding energy (BE) of 284.8 eV, 286.3 eV and 289.1 eV for $\text{C}1s$ peaks were designated to $\text{C}-\text{C}$ group in aliphatic and aromatic fragments [28], $\text{C}-\text{O}$ in $\text{P}-\text{O}-\text{C}$ structures and $\text{C}=\text{O}$ groups oxidized respectively during combustion [29, 30]. As seen in Table 6, it should be noted the percentage of $\text{C}-\text{O}$ groups in EVA/IFR/ZnO residues (7.5%) was higher than that in EVA/IFR residues (6.7%) and this suggested combination of nano-ZnO into IFR system could promote composites forming more $\text{P}-\text{O}-\text{C}$ cross-linking structures. Especially for oxidized carbon atoms ($\text{C}=\text{O}$), the percentage in EVA/IFR/ZnO residues (0.2%) was nearly 12.5 times lower than that in EVA/IFR residues (2.5%), indicating the char barrier effect of the former with the lower oxidation was enough strong to restrain further oxidation of underlying matrix during combustion.

The $\text{O}1s$ fitting curves for the two samples are shown in Fig. 14. The signals at around 531.6 eV showed the existence of $\text{C}=\text{O}$ of phosphate or carbonyl groups while the BE of 533.0 eV should be assigned to $-\text{O}-$ in $\text{P}-\text{O}-\text{C}$ and $\text{C}-\text{O}-\text{C}$ groups [28, 30]. Clearly seen from Table 6, EVA/IFR/ZnO composite possessed the higher percentage

Table 5 Elemental concentrations of EVA/IFR and EVA/IFR/0.5ZnO residues from XPS

Sample	C (wt%)	O (wt%)	N (wt%)	P (wt%)	O/C (%)	N/C (%)	P/C (%)	P/O (%)	P/N (%)
EVA/IFR	33.72	51.08	2.38	12.82	1.51	0.07	0.38	0.25	5.39
EVA/IFR/0.5ZnO	30.82	53.01	2.09	13.24	1.72	0.07	0.43	0.25	6.33

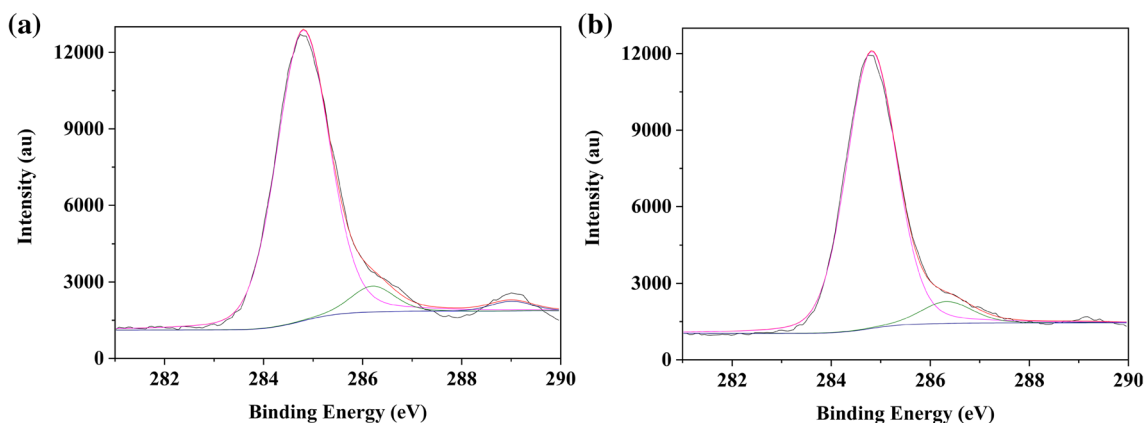


Fig. 13 C1s spectra of char residues of EVA/IFR (a) and EVA/IFR/0.5ZnO (b)

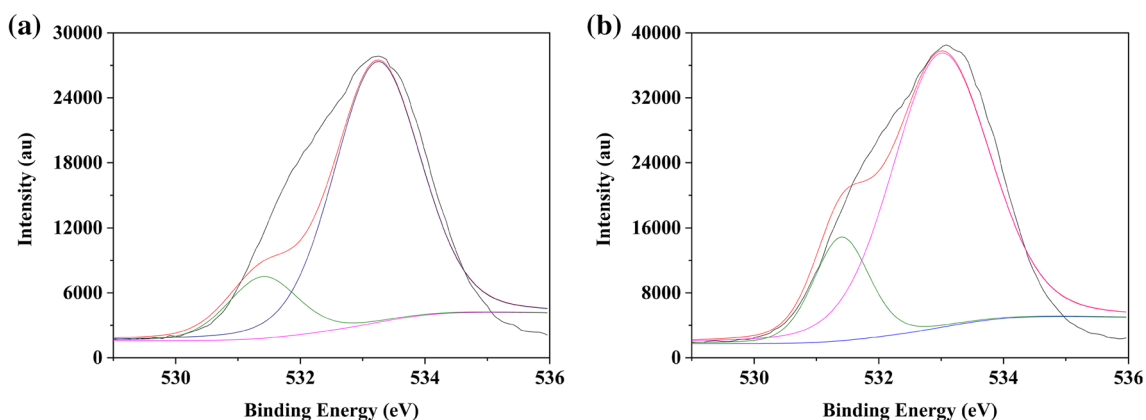


Fig. 14 O1s spectra of char residues of EVA/IFR (a) and EVA/IFR/0.5ZnO (b)

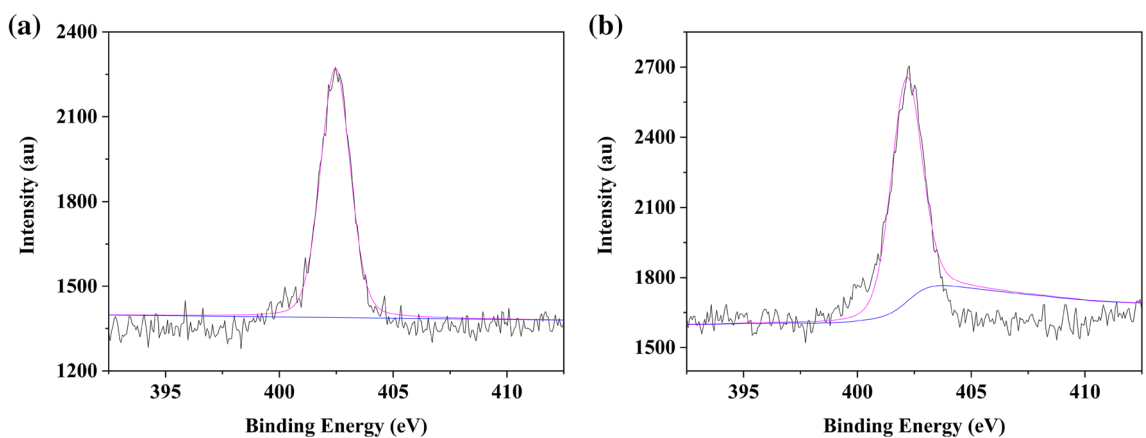


Fig. 15 N1s spectra of char residues of EVA/IFR (a) and EVA/IFR/0.5ZnO (b)

of $-O-$ group (84.1%) than EVA/IFR (82.4%) in residues, which revealed that the introduction of nanometre oxide zinc promoted IFR and EVA matrix forming more cross-linked C–O–C and C–O–P structures during combustion.

Also, the result was in agreement with C1s spectra fitting results.

As seen in Fig. 15, the N1s spectra at 402.0 eV were corresponded to C–N or C=N in the triazine structures, which

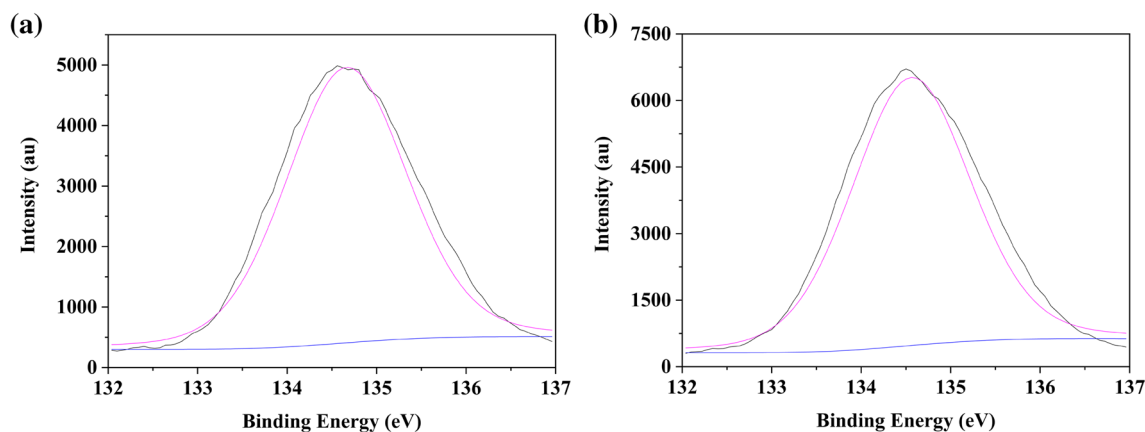


Fig. 16 P2p spectra of char residues of EVA/IFR (a) and EVA/IFR/0.5ZnO (b)

Table 6 Fitting results of C1s, O1s, N1s and P2p spectra for EVA/IFR and EVA/IFR/0.5ZnO residues

	EVA/IFR						EVA/IFR/0.5ZnO					
	Peak-1		Peak-2		Peak-3		Peak-1		Peak-2		Peak-3	
	BE (eV)	Atom %	BE (eV)	Atom %	BE (eV)	Atom %	BE (eV)	Atom %	BE (eV)	Atom %	BE (eV)	Atom %
C1s	284.8	90.8	286.3	6.7	289.1	2.5	284.8	92.3	286.2	7.5	289.0	0.2
O1s	531.4	17.6	533.2	82.4	–	–	531.4	15.9	533.0	84.1	–	–
N1s	402.5	100.0	–	–	–	–	402.2	100.0	–	–	–	–
P2p	134.7	100.0	–	–	–	–	134.6	100.0	–	–	–	–

suggested nitrogen atoms existed in the form of C–N or C=N in residues.

In regard to the spectra of P2p, a single BE peak at 134.7 eV could be owing to P=O structure in P–O–C group. Nevertheless, as known, the P2p peak in the decomposition products (mainly polyphosphoric acid) of APP appeared at 132.8 eV [31]. Thus the shift of bind energy from 132.8 to 134.7 eV indicated the cross-linked reactions among the components containing APP took place, leading to forming C–O–P=O structures [32] in residues after combustion. It may also be concluded that the cross-linking reactions in EVA/IFR/ZnO composite with the addition of nano-ZnO were more efficient than in EVA/IFR proved by the higher P content in residues (Table 5), which was from the phosphorous-containing acids remained in condensed phase during the char-formation process.

Conclusions

The combination of nano-ZnO with IFR system based on APP and triazine char-forming agent HTCFA improved the flame retardant properties and suppressed the combustion

behaviour of EVA with increasing LOI values and reducing the release of heat and smoke by promoting forming superior char layer. Thermal analysis results showed that there was an obvious synergistic effect between nano-ZnO and IFR, and the incorporation of the metal oxide significantly promoted forming more stable char residues of IFR and EVA/IFR. SEM results proved the introduction of nano-ZnO facilitated the formation of a homogeneous and compact intumescent char layer during combustion and this kind of char would play a critical role in condensed-phase flame-retardant mechanism. The residue analysis results indicated nano-ZnO promoted the formation of higher graphitization degree char layer including richer P–O–C and P–N cross-linked structures due to the catalytic carbonization effect of metal oxide and consequently the high-quality char residues more efficiently suppressed the combustion and smoke release of EVA composites. It was concluded that nano-ZnO could be regarded to be an effective synergist enhancing the flame retardant and smoke suppression functions of IFR system based on APP and HTCFA.

Acknowledgements This research was supported by Natural Science Foundation of Beijing Municipality (CN) (2192014).

Compliance with Ethical Standards

Conflict of interest The authors declare that they have no conflict of interest.

References

- Zhang F, Sun WY, Wang Y, Liu BS (2015) Influence of the pentaerythritol phosphate melamine salt content on the combustion and thermal decomposition process of intumescent flame-retardant ethylene-vinyl acetate copolymer composites. *J Appl Polym Sci* 132:42148
- Lu K, Ye LJ, Liang QS, Li YJ (2015) Selectively located aluminum hydroxide in rubber phase in a TPV: towards to a halogen-free flame retardant thermoplastic elastomer with ultrahigh flexibility. *Polym Composite* 36:1258–1265
- Qu HQ, Liu X, Xu JZ, Ma HY, Jiao YH, Xie JX (2014) Investigation on thermal degradation of poly(1,4-butylene terephthalate) filled with aluminum hypophosphite and Trimer by thermogravimetric analysis-Fourier transform infrared spectroscopy and thermogravimetric analysis-mass spectrometry. *Ind Eng Chem Res* 53:8476–8483
- Liu X, Wang JY, Yang XM, Wang YL, Hao JW (2017) Application of TG/FTIR TG/MS and cone calorimetry to understand flame retardancy and catalytic charring mechanism of boron phosphate in flame-retardant PUR-PIR foams. *J Therm Anal Calorim* 130:1817–1827
- Yang W, Hong NN, Song L, Hu Y (2012) Studies on mechanical properties, thermal degradation, and combustion behaviors of poly(1,4-butylene terephthalate)/glass fiber/cerium hypophosphite composites. *Ind Eng Chem Res* 51:8253–8261
- Demir H, Arıkış E, Balköse D, Ülkü S (2015) Synergistic effect of natural zeolites on flame retardant additives. *Polym Degrad Stab* 89:478–483
- Feng CM, Liang MY, Jiang JL, Zhang YK, Huang JG, Liu HB (2016) Synergism effect of CeO₂ on the flame retardant performance of intumescent flame retardant polypropylene composites and its mechanism. *J Anal Appl Pyrol* 122:405–414
- Wang L, Wang W, Wang BB, Wu Y, Hu Y, Song L, Richard KK, Yuen (2012) The impact of metal oxides on the combustion behavior of ethylene-vinyl acetate copolymers containing an intumescent flame retardant. *Ind Eng Chem Res* 51:7884–7890
- Liu Y, Wang Q (2006) Catalytic action of phospho-tungstic acid in the synthesis of melamine salts of pentaerythritol phosphate and their synergistic effects in flame retarded polypropylene. *Polym Degrad Stab* 91:2513–2519
- Estevao LRM, Le Bras M, Delobel R, Nascimento RSV (2005) Spent refinery catalyst as a synergistic agent in intumescent formulations: influence of the catalyst's particle size and constituents. *Polym Degrad Stab* 88:444–455
- Yi JS, Yin HQ, Cai XF (2013) Effects of common synergistic agents on intumescent flame retardant polypropylene with a novel charring agent. *J Therm Anal Calorim* 111:725–734
- Wu N, Yang RJ (2011) Effects of metal oxides on intumescent flame retardant polypropylene. *Polym Adv Technol* 22:495–501
- Jiao C, Zhuo J, Chen X (2013) Synergistic effects of zinc oxide in intumescent flame retardant silicone rubber composites. *Plast Rubber Compos* 42:374–378
- Xu ML, Chen YJ, Qian LJ, Wang JY, Tang S (2014) Component ratio effects of hyperbranched triazine compound and ammonium polyphosphate in flame-retardant polypropylene composites. *J Appl Polym Sci* 131:41006
- Xu B, Ma W, Wu X, Qian LJ, Jiang S (2018) Flame retardancy and thermal behavior of intumescent flame retardant EVA composites with an efficient triazine-based charring agent. *Mater Res Express* 5:045309
- Feng CM, Zhang Y, Liang D, Liu SW, Chi ZG, Xu JR (2013) Flame retardancy and thermal degradation behaviors of polypropylene composites with novel intumescent flame retardant and manganese dioxide. *J Anal Appl Pyrolysis* 104:59–67
- Rimez B, Rahier H, Biesemans M, Bourbigot S, Van Mele B (2015) Flame retardancy and degradation mechanism of poly(vinyl acetate) in combination with intumescent flame retardants: I. Ammonium poly(phosphate). *Polym Degrad Stab* 25:277–292
- Rimez B, Van Assche G, Bourbigot S, Rahier H (2016) Modeled decomposition kinetics of flame retarded poly(vinyl acetate). *Chem J Chin Univ* 20:146–149
- Zanetti M, Camino G, Thomann R, Mülhaupt R (2011) Synthesis and thermal behaviour of layered silicate-EVA nanocomposites. *Polymer* 42:4501–4507
- Riva A, Camino G, Fomperie L, Amigouët P (2003) Fire retardant mechanism in intumescent ethylene vinyl acetate compositions. *Polym Degrad Stab* 82:341–346
- Zanetti M, Kashiwagi T, Falqui L, Camino G (2002) Cone calorimeter combustion and gasification studies of polymer layered silicate nanocomposites. *Chem Mater* 14:881–887
- Feng CM, Zhang Y, Liu SW, Chi ZG, Xu JR (2013) Synergistic effects of 4A zeolite on the flame retardant properties and thermal stability of a novel halogen-free PP/IFR composite. *Polym Adv Technol* 24:478–486
- Nie SB, Hu Y, Song L, He QL, Yang DD, Chen H (2008) Synergistic effect between a char forming agent (CFA) and microencapsulated ammonium polyphosphate on the thermal and flame-retardant properties of polypropylene. *Polym Adv Technol* 19:1077–1083
- Zhou S, Song L, Wang ZZ, Hu Y, Xing WY (2008) Flame retardation and char formation mechanism of intumescent flame retarded polypropylene composites containing melamine phosphate and pentaerythritol phosphate. *Polym Degrad Stab* 93:1799–1806
- Mahapatra SS, Karak N (2007) s-Triazine containing flame retardant hyperbranched polyamines: synthesis, characterization and properties evaluation. *Polym Degrad Stab* 92:947–955
- Ye L, Zhang YJ, Wang SH, Gao GG, Liu JX, Zhou YL, Liu H (2014) Synergistic effects and mechanism of ZnCl₂ on intumescent flame-retardant polypropylene. *J Therm Anal Calorim* 115:1065–1071
- Xu GY, Cheng JY, Wu HY, Lin Q, Zhang YC, Wang H (2013) Functionalized carbon nanotubes with oligomeric intumescent flame retardant for reducing the agglomeration and flammability of poly (ethylene vinyl acetate) nanocomposites. *Polym Composite* 34:109–121
- Peng HQ, Wang DY, Zhou Q, Wang YZ (2008) An S- and P-containing flame retardant for polypropylene. *Chin J Polym Sci* 26:299–309
- Meng FC, Liang MY, Jiang JL, Liu HB, Huang JG (2016) Synergistic effect of ammonium polyphosphate and triazine-based charring agent on the flame retardancy and combustion behavior of ethylene-vinyl acetate copolymer. *J Anal Appl Pyrol* 119:259–269
- Deng CL, Deng C, Zhao J, Li RM, Fang WH, Wang YZ (2015) Simultaneous improvement in the flame retardancy and water resistance of PP/APP through coating UV-curable pentaerythritol triacrylate onto APP. *Chin J Polym Sci* 33:203–214
- Ke CH, Li J, Fang KY, Zhu QL, Zhu J, Yan Q, Wang YZ (2010) Synergistic effect between a novel hyperbranched charring agent and ammonium polyphosphate on the flame retardant

- and anti-dripping properties of polylactide. *Polym Degrad Stab* 95:763–770
32. Strzemieska B, Voelkel A, Donate-Robles J, Martín-Martínez JM (2014) Assessment of the surface chemistry of carbon blacks by TGA-MS, XPS and inverse gas chromatography using statistical chemometric analysis. *Appl Surf Sci* 316:315–323

Publisher's Note Springer Nature remains neutral with regard to jurisdictional claims in published maps and institutional affiliations.